ELSEVIER

Volume 183, Issue 3, March 2010

JOURNAL OF SOLID STATE CHEMISTRY

www.elsevier.com/locate/jssc

# CONTENTS

Abstracted/indexed in BioEngineering Abstracts, Chemical Abstracts, Coal Abstracts, Current Contents/Physics, Chemical, & Earth Sciences, Engineering Index, Research Alert, SCISEARCH, Science Abstracts, and Science Citation Index. Also covered in the abstract and citation database SCOPUS®. Full text available on ScienceDirect®.

## *Regular Articles*



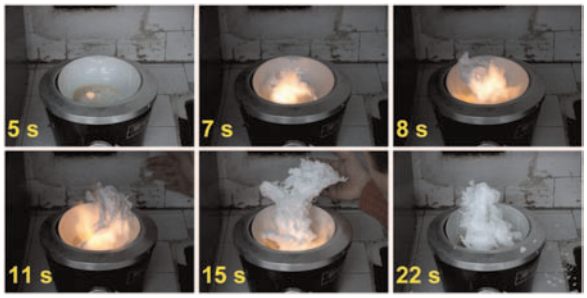


Single-phase $CaZrO_3$ powder was prepared by low-temperature combustion synthesis. The resulting powder had a BET area of 21.5 $m^2$/g. After sintering at 1400 °C for 2 h 95% of the theoretical density was reached.



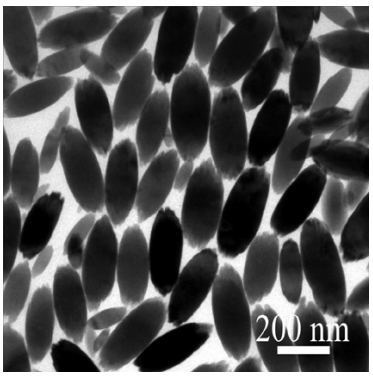


Uniform shuttle-like $Ln^{3+}$($Eu^{3+}$, $Tb^{3+}$) doped $NaLa(WO_4)_2$ nanocrystals have been solvothermally synthesized in the mixed solvent of ethylene glycol (EG) and water at 180 °C for 16 h.

## *Regular Articles—Continued*



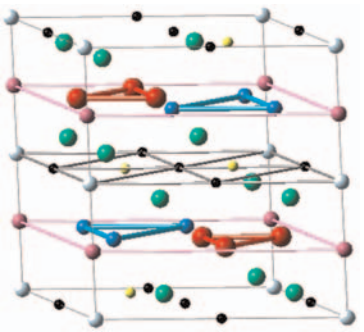

The crystal structure of $R_3T_4Al_{12}$ could be considered as two kinds of layer stacking up along the hexagonal $c$ axis. Fe and Ru atoms preferentially substitute for Al atoms at 6*h* site.



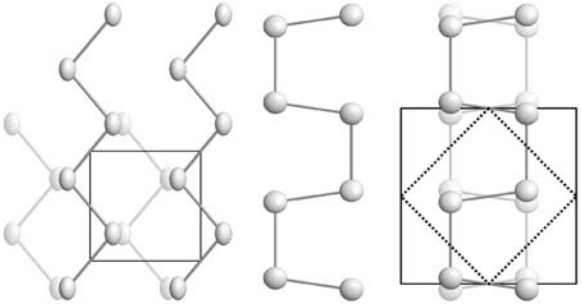

Zigzig vs. cis-trans.

*Continued*

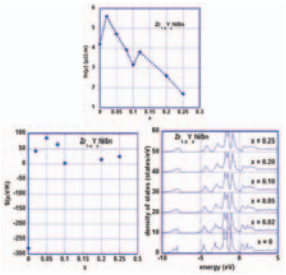

Both approaches experimental and calculations point to the same conclusions. Resistivity and thermopower measurements assert that doping of ZrNiSn based compound by the Y as acceptor impurity induces the insulator–metal transition and leads the $S$ value sign reverse.



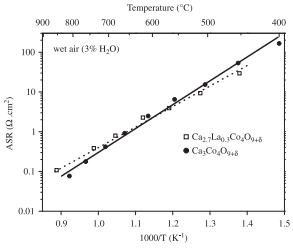


Arrehnius plots of the ASR for $Ca_3Co_4O_{9+\delta}$ and $Ca_{2.7}La_{0.3}Co_4O_{9+\delta}$.



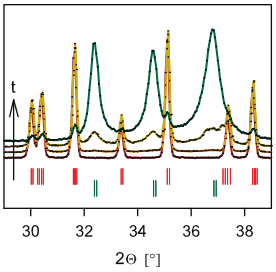


The ammonolysis of $\beta$-$Ga_2O_3$ powders forming GaN at temperatures of 600–780 °C was monitored by means of XRD, neutron diffraction and X-ray absorption spectroscopy in order to identify the possible intermediates and the solubility limit of nitrogen in the oxide lattice.



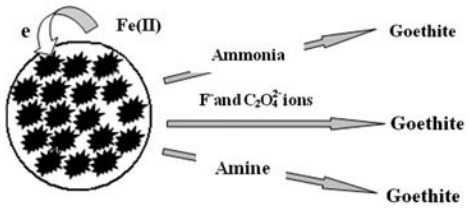


Fe(II)-induced transformation of ferrihydrite in the presence of ammonia, amine and coordination ions of Fe(III) was studied. The introduction of the additives favors the formation of goethite.



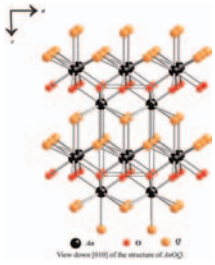

View down [010] of the structure of $AnOQ$.



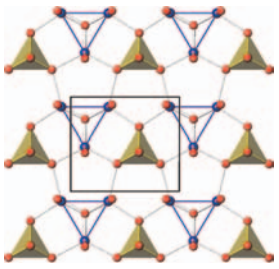

Structural view of a single layer of the triangular lattice of $La_4Cu_3MoO_{12}$ perpendicular to the $b$-axis. The copper atoms are blue, the oxide ions are red and the MoO5 trigonal bipyramids are yellow. The isolated triangular clusters of $Cu_3O$ are outlined by the thin blue lines.

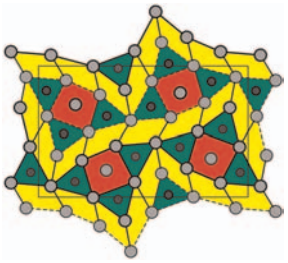

$Hf_{3\pm\delta}Nb_{4\pm\delta}As_3$ (*Pnma*, new structure type) is stabilized by differential fractional site occupation. Its structural relations within a homologous series based on W-type, Mg-type and $Al_2B$-type building blocks are discussed.



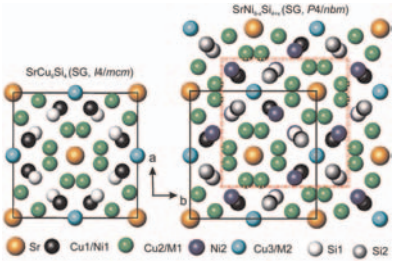


The crystal structure of $SrNi_{9-x}Si_{4+x}$ (own-type, $x = 2.7$, $a = 0.78998(3)$, $c = 1.1337(2)$ nm; space group $P4/nbm$) was determined from X-ray single crystal counter to be a low symmetry derivative of the cubic, parent $NaZn_{13}$-type and is related to $CeNi_{8.5}Si_{4.5}$-type.



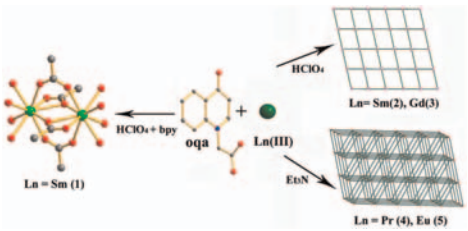


The hydrothermal reactions of the oqa molecules with varied lanthanide ions resulted in the formation of five new complexes, which exhibit three typical structure features.



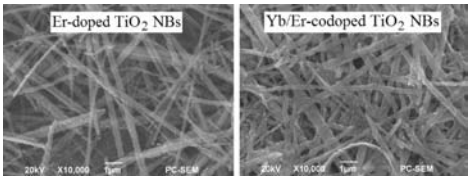


Anatase $TiO_2$ nanobelts doped with $Er^{3+}$ or $Yb^{3+}/Er^{3+}$ cations were simply synthesized using two-step preparation proceedings of ion-exchange and hydrothermal treatment, and their upconversion emissions were also investigated. SEM images of $TiO_2$ nanobelts (NBs) doped with $Er^{3+}$ (the left) and codoped with $Yb^{3+}/Er^{3+}$ (the right).



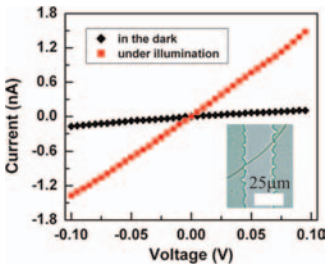


The Schiff base zinc nanoribbons nanowires exhibited good photoresponse under an incandescent lamp, which indicated their potential application as organic semiconductive or photoconductive nanodevices in the future.



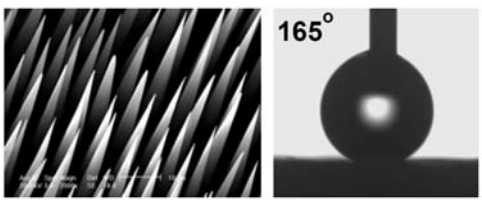


Silica needle arrays are fabricated by tube arrays fabrication and etching method. They show super hydrophobic property after being treated with PDMS.

*Continued*

**A Facile synthesis of flower-like $Co_3O_4$ porous spheres for the lithium-ion battery electrode**
Jun Zheng, Jing Liu, Dongping Lv, Qin Kuang, Zhiyuan Jiang, Zhaoxiong Xie, Rongbin Huang and Lansun Zheng
***Page 600***

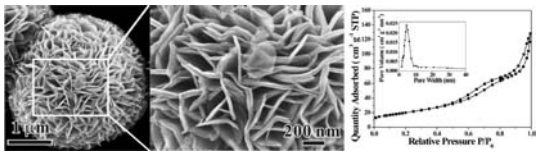


The flower-like $Co_3O_4$ porous spheres with hierarchical structure have been successfully prepared via a simple calcination process using cobalt hydroxide as precursor.

---

**Synthesis, crystal structure, and properties of the rhombohedral modification of the thiospinel $CuZr_{1.86(1)}S_4$**
Yongkwan Dong, Michael A. McGuire, Hoseop Yun and Francis J. DiSalvo
***Page 606***

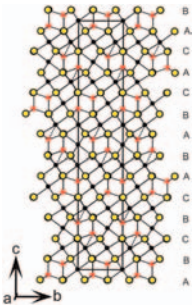


The projected view of the rhombohedral modification, $CuZr_{1.86(1)}S_4$, down the [100] direction. Large letters denote the packing sequence of the S atoms (yellow circles) along the *c* axis. Zr (black circles) and Cu (red circles) atoms occupy the octahedral and tetrahedral holes, respectively, between close packed S layers.

---

**The effect of low levels of dopants upon the formation and properties of beta-phase molybdenum nitride**
A.G. Cairns, J.G. Gallagher, J.S.J. Hargreaves, D. Mckay, J.L. Rico and K. Wilson
***Page 613***

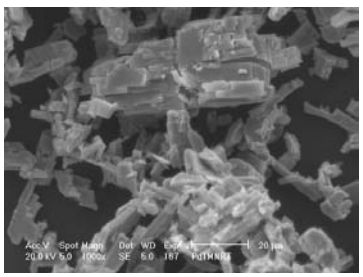

Low levels of Pd, Au, Ni and Cu dopant have significant effects upon the morphology, formation and dentitridation characteristics of beta-phase molybdenum nitride.

**Luminescence enhancement of $Eu^{2+}$, $Ce^{3+}$ co-doped $Ba_3Si_5O_{13-\delta}N_\delta$ phosphors**
Ruili Zhang, Tomonori Maeda, Ryosuke Maruta, Sho Kusaka, Bingjun Ding, Kei-ichiro Murai and Toshihiro Moriga
***Page 620***

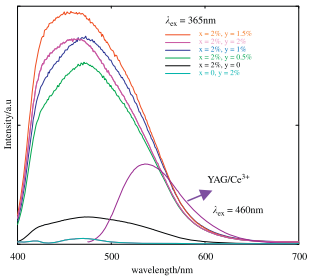


Emission spectra for $Ba_{3(1-x-y)}Si_5O_{13-\delta}N_\delta/xEu^{2+},yCe^{3+}$ ($0 \le x \le 2\%$, $0 \le y \le 2\%$) under the excitation wavelength of 365 nm.

---

**New high permittivity tetragonal tungsten bronze dielectrics $Ba_2LaMNb_4O_{15}$: $M$ = Mn, Fe**
Emma E. McCabe and Anthony R. West
***Page 624***

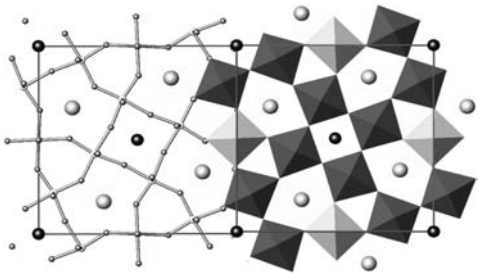

Tetragonal tungsten bronze structure of $Ba_2La(Mn, Fe)Nb_4O_{15}$ from two different viewpoints.

---

**Solution precursor synthesis and magnetic properties of $Eu_{1-x}Ca_xTiO_3$**
Nathaniel L. Henderson, Xianglin Ke, Peter Schiffer and Raymond E. Schaak
***Page 631***

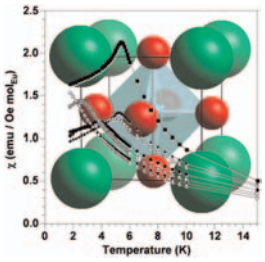


Twelve members of the $Eu_{1-x}Ca_xTiO_3$ solid solution ($0 \le x \le 1$) were synthesized by first forming a homogeneously mixed precursor using a modified sol–gel process, followed by reductive annealing. Samples with $x \le 0.60$ are antiferromagnetic, with $T_N$ decreasing as the level of calcium substitution increases.

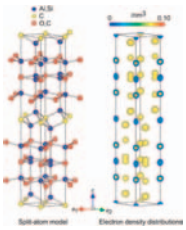

A new oxycarbide discovered in the Al–Si–O–C system, $Al_4SiC_4$-homeotypic $[Al_{4.4}Si_{0.6}][O_{1.0}C_{2.0}]C$. The crystal is an inversion twin, and hence the structure is represented by a split-atom model. The three-dimensional electron density distributions are determined by the maximum-entropy methods-based pattern fitting, being consistent with the disordered structural model.



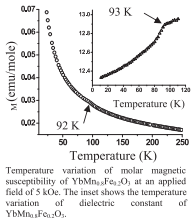


Temperature variation of molar magnetic susceptibility of $YbMn_{0.5}Fe_{0.5}O_3$ at an applied field of 5 kOe. The inset shows the temperature variation of dielectric constant of $YbMn_{0.5}Fe_{0.5}O_3$.

Hexagonal manganites of the type $YbMn_{1-x}Fe_xO_3$; $x \leq 0.3$ have been synthesized by the solid state route. The distortion of the $MnO_5$ polyhedra (tbp) decreases and the Mn–O–Mn bonds in the *a*–*b* plane become shorter with Fe-substitution. The compounds were found to be antiferromagnetic and the ordering temperature $T_N$ increased from 82 K for pure $YbMnO_3$ to 95 K for $YbMn_{0.7}Fe_{0.3}O_3$. The increase in the ordering temperature in $YbMn_{1-x}Fe_xO_3$ is explained on the basis of increase in covalence of Mn/Fe–O–Mn/Fe bonds with iron substitution. Low temperature dielectric measurements show a unique correlation between the magnetic and electric fields for all compositions.



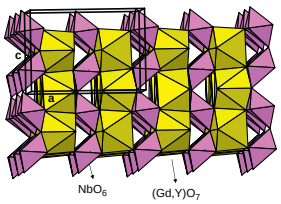


Crystal structure for $(Gd_xY_{3-x})NbO_7$ showing the partial layered feature. The alternate stacking of distorted $NbO_6$ octahedra and $(Gd,Y)O_7$ polyhedra are illustrated. The $(Gd,Y)O_8$ polyhedra are omitted for clarity.



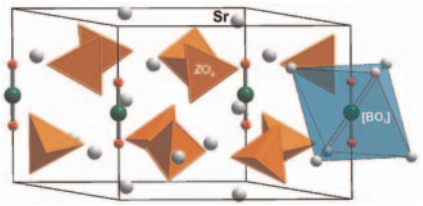


Single crystals of the strontium phosphate orthoborate metaborate, $Sr_{10}[(PO_4)_{5.5}(BO_4)_{0.5}](BO_2)$, were grown from the melt and structurally characterized. The crystal structure is closely related to apatite and contains uncommon linear $[BO_2]^-$ metaborate groups taking positions within the channels running along the three-fold inversion axis.



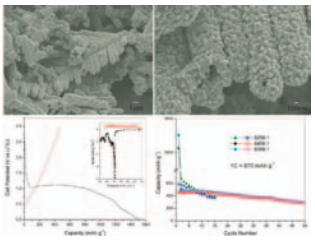

SEM images of 3D dendrite-shaped CuO hollow micro/nanostructures prepared *via* a Kirkendall-effect-based approach have been shown. The as-prepared CuO electrode exhibited significantly improved cyclability for Li-ion batteries.



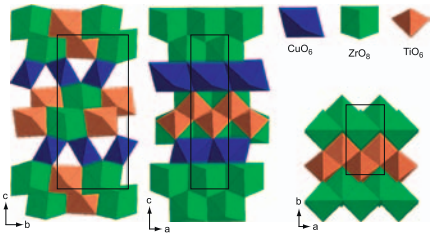


The new compound $CuZrTiO_5$ is orthorhombic ($P2_12_12_1$), with $a = 3.5871(3)$ Å, $b = 6.6968(4)$ Å, $c = 14.6679(9)$ Å. The structure, determined with single crystal XRD, represents a new crystal structure type that is a slight distortion of that of $In_2TiO_5$ but differs in space group and cation coordination.

*Continued*

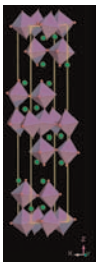

The magnetic structures of $Ca_4Mn_{3-x}Ta_xO_{10}$ transit from G-type AFM to cluster glass state with the intermediate state of FM clusters exhibited in AFM matrix as Ta increasing.



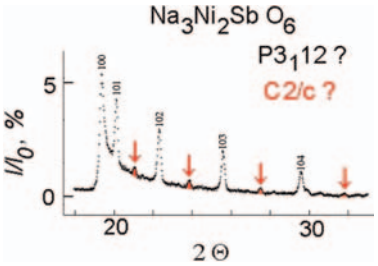


It is shown that the powder patterns for $Na_3M_2SbO_6$ ($M$ = Ni and Co) may be equally well described by a trigonal $P3_112$ cell and a monoclinic $C2/m$ cell. In addition, the Ni compound exhibits a series of extremely weak reflections ($I<0.3\%$) that need doubling of the monoclinic $c$ axis, and the final cell is $C2/c$.



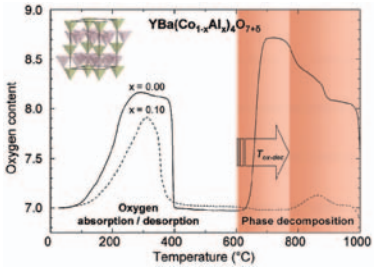


A small amount of aluminum replacing cobalt in $YBaCo_4O_{7+\delta}$ works efficiently for boosting up the phase-decomposition temperature ($T_D$), but yet retains the unique low-temperature oxygen-storage characteristics of the phase.



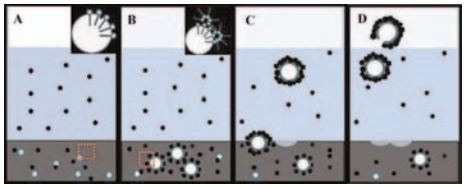


A proposed growth mechanism of large scale hollow ZnO. Bubbles provide the aggregation center for ionic liquids that leads to the formation of hollow Zn particle-dotted shells, buoyancy promotes shells to go upward, the breach occurs when shells are subjected to overpressure.



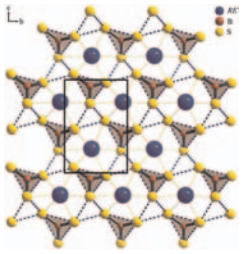

The isotypic orthothioborates Ce[$BS_3$], Pr[$BS_3$] and Nd[$BS_3$] were prepared using different preparation routes. The crystal structure of the title compounds was determined from X-ray powder diffraction data. The crystal structures contain isolated $[BS_3]^{3-}$ groups with boron in trigonal-planar coordination. The sulfur atoms form the vertices of corrugated kagome nets (sketched with blue dotted lines), which are stacked along [100] according to the sequence ABAB. Within these nets every second triangle is occupied by boron and the large hexagons are centered by rare earth ions, which are surrounded by overall nine sulfur species.



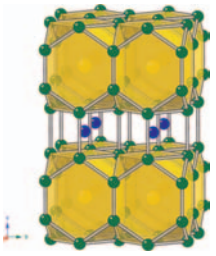

The compound $CePd_{1+x}Al_{6-x}$ ($x=0.5$) has been synthesized and structurally characterized by single-crystal X-ray diffraction. The measured physical properties of temperature and field dependent magnetic susceptibility, specific heat, and electrical resistivity suggests that the compound undergoes ferromagnetic order at *ca.* 2.8 K and further exhibits relatively heavy fermion behavior with a Sommerfeld coefficient of 500 mJ/mol-K2.

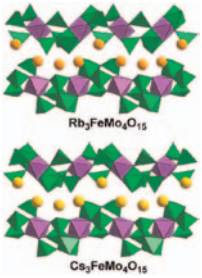


Systems $M_2MoO_4$–$Fe_2(MoO_4)_3$ ($M$ = Rb, Cs) are non-quasibinary joins of the systems $M_2O$–$Fe_2O_3$–$MoO_3$ where new compounds $M_3FeMo_4O_{15}$ were revealed. Their structures have diverse mutual arrangements of the adjacent chains of $Fe^{3+}O_6$, $MoO_6$ and $MoO_4$ polyhedra.



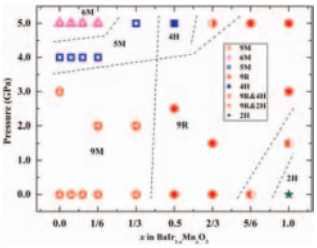


The $BaRu_{1-x}Mn_xO_3$ solid solutions were synthesized by using the solid-state chemical method and high-pressure sintering, and the pressure–composition "phase diagram" at 1000 °C was obtained.



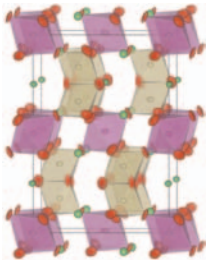

Structure of $Ba_3BiIr_2O_9$ at 300 K. $BiO_6$ octahedra are purple, $IrO_6$ octahedra are gold, and Ba atoms are green. Thermal ellipsoids at 90% probability.



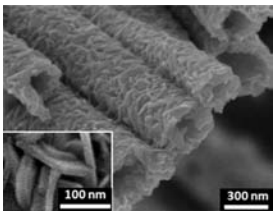


This paper described a simple and convenient approach that allows for the facile fabrication of $BaFe_{12}O_{19}$ hierarchical nanotubes or nanotube arrays by a deliberately devised two-step heat-treatment process, in which the dense shells generated in situ during the short-time pre-treatment procedure direct Ostwald ripening of flake-shaped $BaFe_{12}O_{19}$ nanocrystals in the elevated temperature heat-treatment procedure.



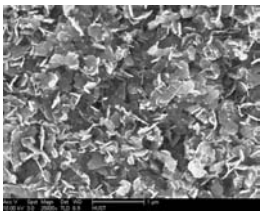

$Mn_3O_4$ hexagonal nanoplates and nanoparticles were synthesized via a solvent-assisted hydrothermal oxidation process at low temperature and a solvothermal oxidation method, respectively. Their capability of catalytic oxidation of aldehyde at room temperature and atmospheric pressure and electrochemical properties by cyclic voltammogram were compared.



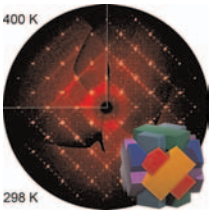


Reciprocal layer $hk0$ for the orthorhombic room temperature phase, with pseudo cubic symmetry due to twinning, and the cubic high temperature phase of $CsFeO_2$. Upon heating the major structural changes are driven by the enhancement of librational motion of the $[FeO_{4/2}]^-$ corner-sharing tetrahedra, a phenomenon related to the high/low phase transition of cristobalite.

*Continued*

## Author inquiries

For inquiries relating to the submission of articles (including electronic submission where available) please visit this journal's homepage at http://www.elsevier.com/locate/jssc. You can track accepted articles at http://www.elsevier.com/trackarticle and set up e-mail alerts to inform you of when an article's status has changed. Also accessible from here is information on copyright, frequently asked questions and more.
Contact details for questions arising after acceptance of an article, especially those relating to proofs, will be provided by the publisher.

**Language services.** Authors who require information about language editing and copyediting services pre- and post-submission please visit http://www.elsevier.com/locate/languagepolishing or our customer support site at http://epsupport.elsevier.com. Please note Elsevier neither endorses nor takes responsibility for any products, goods or services offered by outside vendors through our services or in any advertising. For more information please refer to our Terms & Conditions http://www.elsevier.com/termsandconditions

For a full and complete Guide for Authors, please go to: http://www.elsevier.com/locate/jssc

*Journal of Solid State Chemistry* has no page charges.